Nanoscience and Nanotechnology Letters
Vol. 7, 920–929, 2015

Formation of Non-Toxic Au Nanoparticles with Bimodal Size Distribution by a Modular Redesign of Ultrasonic Spray Pyrolysis

Peter Majerič[1,*], Darja Jenko[2], Bojan Budič[3], Sergej Tomić[4], Miodrag Čolić[5], Bernd Friedrich[6], and Rebeka Rudolf[1,7]

[1] *University of Maribor, Faculty of Mechanical Engineering, Smetanova ulica 17, 2000 Maribor, Slovenia*
[2] *Institute of Metals and Technology, IMT, Lepi pot 11, 1000 Ljubljana, Slovenia*
[3] *National Institute of Chemistry, Hajdrihova 19, 1001 Ljubljana, Slovenia*
[4] *Institute of Medical Research, Military Medical Academy, Crnotravska 17, 11000 Beograd, Serbia*
[5] *Medical Faculty, University of Nis, Bulevar Dr Zorana Đinđića 81, 18000 Niš, Serbia*
[6] *IME Institute of Process Metallurgy and Metal Recycling, RWTH Aachen, Intzestraße 3, 52056 Aachen, Germany*
[7] *Zlatarna Celje d.d., Kersnikova 19, 3000 Celje, Slovenia*

This article reports about a new synthesis approach by the Ultrasonic Spray Pyrolysis of Au nanoparticles which consists of a separate heating zone for evaporation and subsequent connection of reduction gas by entering directly into the reaction zone. This redesign was made in order to control each step of the USP to find those influential parameters which dictate final gold nanoparticles' morphology and size. For the precursor a starting solution of $HAuCl_4$ and water was used with various concentrations of Au (0.625 g/l, 1.25 g/l and 2.5 g/l). Other variable parameters were evaporation temperatures (75 °C, 80 °C and 85 °C) and time of synthesis (3 h, 6 h, 9 h), while the temperature in the heating zone was constant (350 °C) during performing all the experiments. Characterization of synthesized Au nanoparticles was carried out by Transmission Electron Microscopy (TEM). It was found that Au nanoparticles have bimodal size distribution. An investigation of the Au nanoparticles' electron diffractions enabled us to find the possible growth of Au nanocrystal types which was finally the base for setting up the synthesis mechanisms of Au nanoparticles. The cytocompatibility investigations of the Au nanoparticles suggested that they were not cytotoxic for L929 cells *in vitro*, but they can exhibit anti-proliferative properties, depending on their size distribution.

Keywords: Ultrasonic Spray Pyrolysis (USP), Gold Nanoparticles, Transmission Electron Microscopy (TEM), Bimodal Particle Size Distribution, Nanoparticle Characterization, Cytocompatibility.

1. INTRODUCTION

The potential benefits of Au nanoparticles (AuNPs) used in medicine attract considerable attention in the scientific community.[1–6] The exploitation of surface plasmon resonance, ease of surface functionalization and biocompatibility that AuNPs inherit can aid the current methods for diagnosis and treatment substantially.[7–11] Pre-clinical proofs of the concept of treatments using nanoparticles have already been established.[12] Currently there is a need for a scaled up production of nanoparticles, able to take up generation of the quantities of nanoparticles required for clinical testing. Technologies for generating nanoparticle powders and suspensions have been existent for several decades[13] and are continuing to being improved upon, while novel approaches are also being studied,[14,15] mostly because the former method produces large batch-to-batch variations in the AuNPs' properties. One such method for the synthesis of AuNPs is the Ultrasonic Spray Pyrolysis (USP).[16] This process is considered to be relatively cost-effective and easily scalable from the laboratory to an industrial level. Several different types of nanoparticles can be produced with this process, as we showed for Au,[16] Ag,[17] TiO_2,[18] etc. Furthermore, by the modifications to the process, several different structure types can also be produced, such as solid or hollow nanoparticles, core–shell and ball-in-ball structures, etc.[19–23]

*Author to whom correspondence should be addressed.

 1941-4900/2015/7/920/010 doi:10.1166/nnl.2015.2046

USP produces AuNPs from a precursor solution with dissolved hydrogen tetrachloroaurate ($HAuCl_4$).[16] We showed previously that USP is able to generate highly purified AuNPs, even from gold scrap.[24] Furthermore, we showed that such pure AuNPs are not cytotoxic for L929 cells, rat thymocytes[25] and splenocytes,[24] up to a concentration of 100 μg/ml. However, with the conventional USP, various types of AuNPs have been obtained (irregular, spherical, triangular, cylindrical),[16] with little control over the synthesis process.

In order to improve the synthesis procedure of AuNPs and produce more uniform spherical nanoparticles, a modular redesign of the USP device was introduced in this paper, to separate the evaporation stage from the rest of the synthesis stages. Our goal was to determine the effects of such an approach on AuNPs' size and morphology. A theoretical calculation used previously with conventional USP was also made to predict the properties of the obtained AuNPs and check for the usefulness of such a calculation and comparison with the new approach on an experimental level. Additionally, we aimed to assess the cytotoxicity and functional properties of such AuNPs *in vitro* using L929 cells, which are recommended by the ISO Standards for the biocompatibility testing of medical devices.

2. EXPERIMENTAL PROCEDURE

2.1. Modular Redesign of USP for AuNP Synthesis

The existing USP device at the IME Institute of Recycling and Processes at RWTH University in Aachen (Germany) was redesigned with a modular separate heating zone in order to divide the aerosol droplet evaporation and particle drying from the rest of the synthesis stages (Fig. 1). An ultrasonic nebulizer Gapusol RBI 9000 (France) with an ultrasound frequency of 2.5 MHz was used to produce aerosol droplets. The precursor solutions were prepared with $HAuCl_4$ diluted with water, where different concentrations of Au were used (2.5, 1.25 and 0.625 g/l) (Table I). The tube diameter was 20 mm. Two tube furnaces were used for the evaporation and reaction heating zones (both 28 cm in length), and the temperature of the first heating zone was varied in the experiments (Table I), while the second heating zone remained constant (350 °C). The first heating zone temperatures were selected in accordance with the calculations presented in Xiong and Kodas,[26] Kodas and Hampden-Smith,[22] Jayanthi et al.[27] and were kept below 100 °C. The calculation of temperature for evaporation was based on a droplet of the starting solution, with selected concentrations, of a diameter of 10 μm. The droplet evaporation was to be finished at the end of the evaporation zone (28 cm, retention time 3.5 seconds). The diffusion of solute into the droplet center is, therefore, given the highest amount of time in the given system, which favors the formation of spherical nanoparticles. It was calculated that evaporation of droplets and super saturation of gold chloride was favorable for solid spherical nanoparticle synthesis with evaporation temperatures of 75, 80 and 85 °C for Au concentrations in precursor solutions of 2.5, 1.25 and 0.625 g/l, respectively. In our previous research,[28] we have synthesized nanoparticles with varying Au concentrations in precursor solutions, from 0.5 to 5.0 g/l and evaporation temperatures from 60 to 150 °C. In this work, the temperatures selected in Table I were deemed as most favorable for the given concentrations. The second heating zone temperature of 350 °C was selected with regard to the temperatures required for $HAuCl_4$ thermal decomposition and hydrogen reduction in previous successful experiments with conventional USP.[16]

Nitrogen (N_2) was used as the carrier gas for aerosol droplets and hydrogen (H_2) was introduced into the system

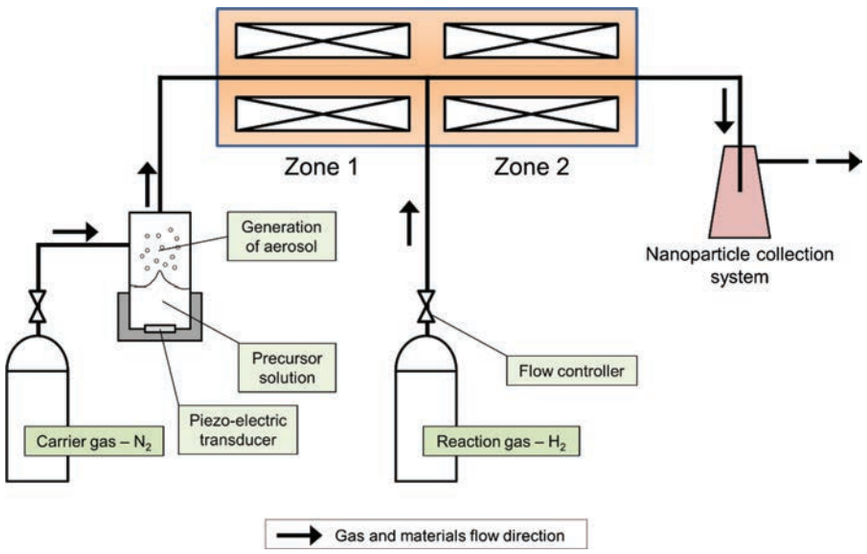

Fig. 1. Schematic diagram of the modular redesign of the USP system.

Table I. Experiment parameters.

Experiment	Au concentration in precursor solution (g/l)	First heating zone temperature (°C)	Second heating zone temperature (°C)	Time of synthesis (h)
Exp. 1	2,5	75	350	3
Exp. 2	1,25	80	350	6
Exp. 3	0,625	85	350	9

as the reduction gas before the second heating zone, for gold chloride reduction into pure AuNPs. The N_2 gas flow was 1.5 l/min, while the H_2 gas flow was kept at 1.0 l/min. The collection bottles for AuNPs were filled with deionized (DI) water, and the AuNPs were gathered in them after 3, 6 or 9 h, as indicated in Table I. The time of synthesis was longer for the experiments with lower Au concentrations in the precursor solution to produce similar quantities of the final product in each experiment.

2.2. Characterization of AuNPs Produced by USP

Conventional Transmission Electron Microscopy (CTEM; JEOL 2100), High-Resolution Transmission Electron Microscopy (HRTEM; JEOL 2100), Electron Diffraction (ED/TEM; JEOL 2100), Energy Dispersive Spectroscopy (EDS/TEM; JED-2300) and Optical Emission Spectrometry with Inductively Coupled Plasma (ICP-OES; Agilent 720) investigations were conducted on the samples prepared in experiments 1, 2 and 3. The AuNPs' sizes for each experiment were determined from a set of 10 TEM micrographs using ImageJ software,[29] with samples of approximately 500 nanoparticles per particle size distribution.

2.3. Preparation of AuNPs for Cytocompatibility Assays

Prior to the cytocompatibility assays, AuNP solutions were concentrated 150× by centrifuging the primary AuNP solutions at 5000 rpm for 20 minutes. The concentrated solutions were sonicated afterwards for 15 minutes in an ultrasonic bath prior to their use. Control solutions contained Millipore water only, and were prepared following the same procedure.

2.4. Cells Cultures

L929 cells were obtained from ATCC (Washington DC, USA). The cells were propagated in a complete RPMI medium supplemented in 10% fetal calf serum (FCS, Sigma Aldrich, Munich, Germany), 2-mercaptoethanol (2-ME, Sigma), 2 mM L-glutamine (Sigma) and antibiotics (penicillin, streptomycin, gentamicin, 1% each (Galenika, Zemun, Serbia)) in an incubator with 5% CO_2 at 370 °C. For the cytotoxicity assays, L929 cells (0.5×104) were seeded in 96-wells plate in 200 μl of the complete RPMI medium for 4 h. After that, the cells were treated with AuNPs at different concentrations (12 μg/ml–100 μg/ml) or corresponding control solutions (distilled water) for the following 48 h. The cell cultures were monitored regularly by the Phase Contrast Microscope (Olympus, IX51).

2.5. Cytotoxicity Assays

The viability of L929 cells after the cultures was assessed by a Trypan Blue exclusion assay.[24, 25] Briefly, the cells were harvested by trypsinization (0.2% trypsin (Serva, Heidelberg, Germany)/0.02% NaEDTA (Sigma) in RPMI), washed in a complete medium at 1400 rpm for 10 minutes, and then stained with 1% Trypan Blue. The positive cells, identified by light microscopy, were considered as dead, predominantly necrotic cells. The percentages of dead cells were determined on the basis of at least 500 total cells from one well. The percentage of viable cells was calculated as 100% of total cells-% of dead cells. All results were expressed as a mean of triplicates.

Apoptosis was detected by using Propidium Iodide (PI) (Sigma) and flow cytometry, as we described previously.[25] The method is based on the detection of DNA fragmentation as revealed by the quantification of the cells with a hypodiploid amount of DNA. For this purpose L929 cells were harvested, washed with PBS and incubated in 500 μl of PI (10 μg/ml) dissolved in a hypotonic solution (0.1% sodium citrate/0.1% Triton-X solution in distilled water). The cells were incubated for 4 h at room temperature and then analyzed by flow cytometry (Partec Cube 6, Bornbarch, Germany).

2.6. Proliferation Assay

L929 cells were cultivated in the presence of AuNPs or corresponding control solutions, as described for 48 h. During the last 18 h of incubation, the cells were pulsed with 1 μCi/well (3H)-thymidin (6.7 Ci/mmol, Amersham, Bucks, UK). At the end of incubation time the cultures were treated with 0.2% trypsin in order to detach the cells from the plastic surface. After harvesting, the radioactivity was counted using a scintillation counter (Beckman). The results were expressed as mean counts per minute (CPM) of sixplicates.

2.7. Statistics

All experiments were repeated at least 3 times, and the data were analyzed for significant differences using one-way ANOVA since the data followed the Gaussian distribution according to the Kolmogorov-Smirnov test (with Dallal-Wikinson-Lilefor P value). A P value of <0.05 was considered statistically significant.

3. RESULTS AND DISCUSSION

3.1. Effects of Temperature and Precursor Concentration on AuNP Sizes and Morphology

Starting Au concentrations in the precursor solution and aerosol droplet size determine the rate of evaporation

and diffusion (along with other factors: temperature, gas flow, tube diameter, relative humidity). The rate of droplet evaporation can determine the shape of the product and can lead to solid, hollow and irregular shapes of nanoparticles.[27,30] Based on these studies, a slower evaporation time enables the solute to diffuse into the center of the droplet during evaporation and produce solid nanoparticles. For this purpose, the evaporation stage was divided into a separate heating zone, before the introduction of hydrogen gas for the reduction of gold chloride. Therefore, by using low temperatures in the first heating zone, the premature thermal decomposition of the solute was prevented, and it allowed a slower evaporation time. An aerosol generator with an ultrasound frequency of 2.5 MHz was used for all the experiments. The generated droplet sizes were in the same size range for all three experiments, ranging from 1 to 15 μm.[31] As the varied starting concentrations were low (2.5, 1.25, 0.625 g/l) in order to obtain nanoparticles, they did not change the generated droplet sizes between the experiments significantly, as the precursor solutions were very diluted. The final nanoparticle properties were thus determined by the temperatures in the first heating zone and starting concentrations of Au in the precursor solution.

The obtained nanoparticles in the experiments had a bimodal size distribution (Figs. 2 and 3), which presents a new finding in our research of AuNP synthesis with USP. Namely, the AuNPs in exp. 1 had a number size distribution with 38.5 ± 24.5 nm (14–63 nm, 71% of the total AuNP number) and 211 ± 91 nm (120–302 nm, 29% of the total AuNP number) (Fig. 2). In exp. 2 the sizes were 11 ± 7 nm (4–18 nm, 81% of the total AuNP number) and 115 ± 65 nm (50–180 nm, 19% of the total AuNP number) (Fig. 3). In exp. 3, a bimodal distribution is not as apparent, as there is no clear gap between the smaller and larger nanoparticle size group (Fig. 4), sizes of 66.5 ± 53.5 nm (13–120 nm) were obtained.

Previously, we have obtained spherical and irregular nanoparticles within a certain size range.[24,25] The larger, somewhat irregular nanoparticles obtained in the experiments are accompanied by much smaller particles with spherical morphologies (Figs. 2–4).

3.2. AuNP Formation Mechanisms

From literature, it is seen that much smaller nanoparticles are obtained by Gas-To-Particle (GTP) mechanisms, while larger nanoparticles are obtained by Droplet-To-Particle (DTP) synthesis mechanisms in spray pyrolysis.[22] The obtained bimodal particle size distribution is most probably caused by a combination of the DTP and GTP mechanisms. This combination of mechanisms makes controlling the synthesized nanoparticle sizes and morphologies more difficult. To determine which mechanism (DTP or GTP) used more gold content from the precursor solution in order to produce AuNPs we have compared the volume of AuNPs of smaller sizes versus the volume of larger nanoparticle sizes. The number size distributions show a greater number of smaller AuNPs (from 71% to 81% of

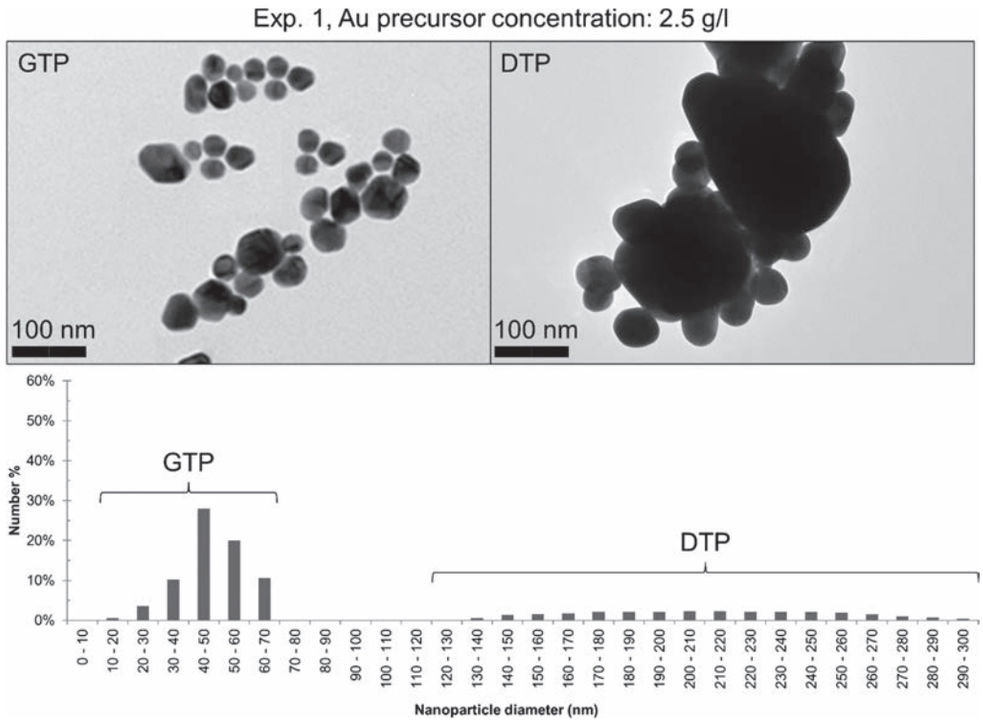

Fig. 2. Bimodal size distribution of AuNPs obtained with the modular USP redesign with accompanying TEM micrographs for exp. 1.

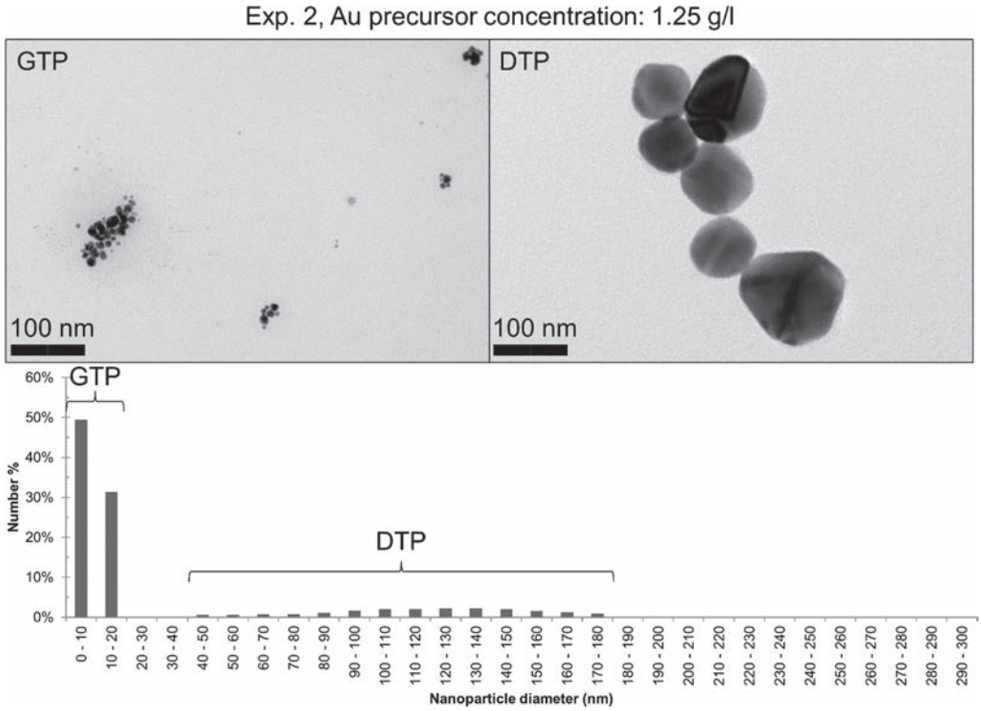

Fig. 3. Bimodal size distribution of AuNPs obtained with the modular USP redesign with accompanying TEM micrographs for exp. 2.

the total AuNPs, for experiments 1 and 2, presented in the previous Chapter) than in the volume size distributions in Figure 5. In the volume size distributions, a lesser percentage of the smaller nanoparticles in experiment 1 (3.6% of the total volume for sizes 38.5 ± 24.5 nm) is shown than for the larger particles (96.4% of the total volume for sizes 211 ± 91 nm). A lesser percentage of the smaller nanoparticles is apparent in experiment 2 (7.6% of

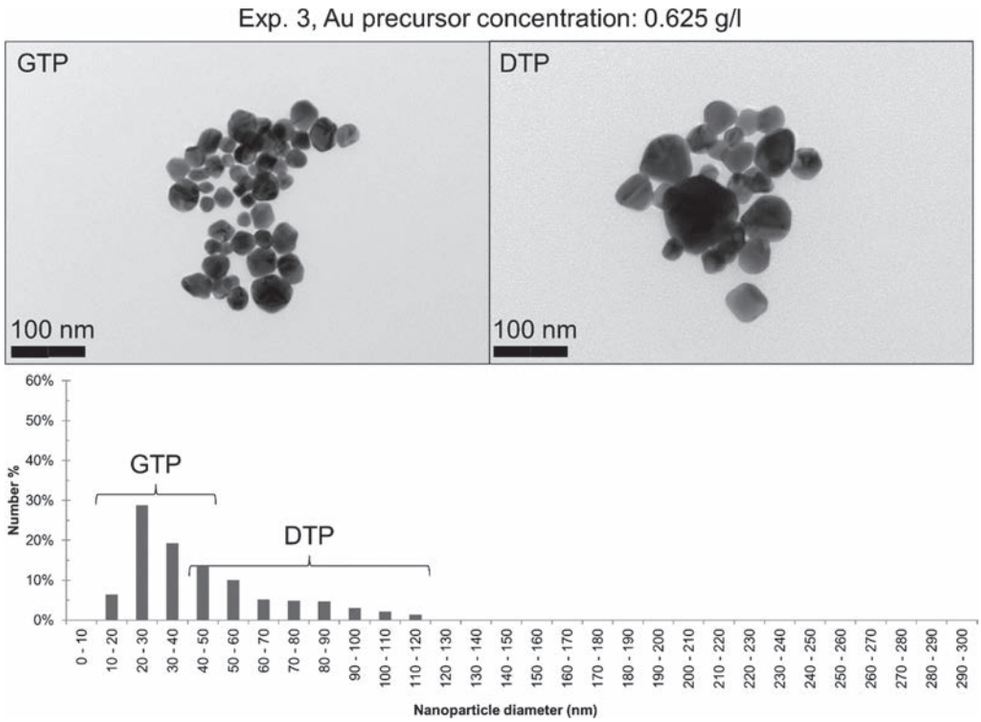

Fig. 4. Size distribution of AuNPs obtained with the modular USP redesign with accompanying TEM micrographs for exp. 3.

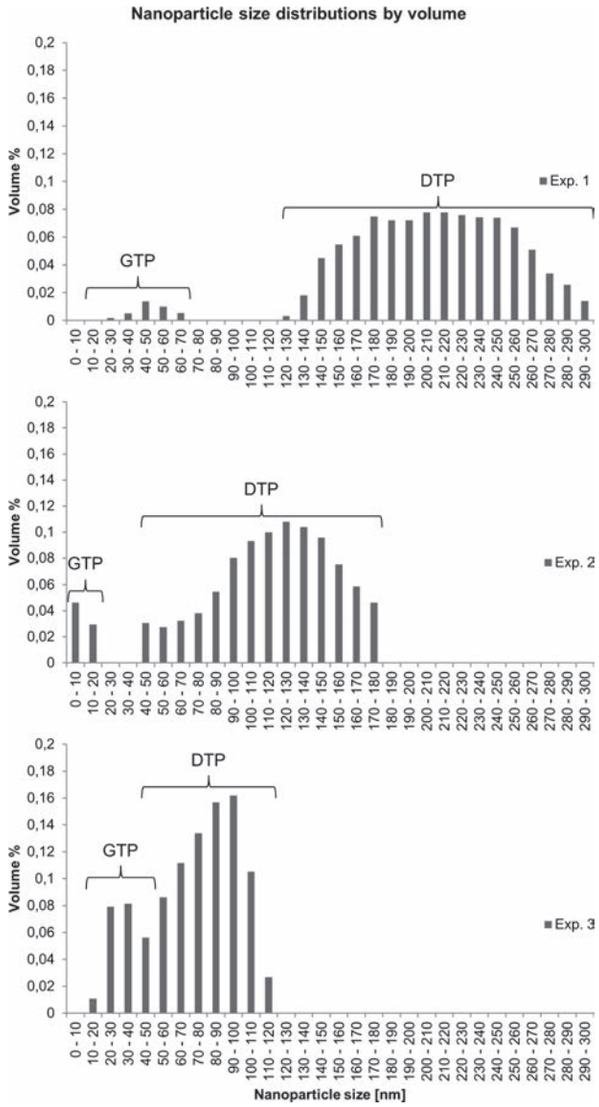

Fig. 5. AuNP bimodal size distributions of experiments *by volume*.

the total volume for sizes from 11 ± 7 nm) and a much greater percentage for the larger nanoparticles (92.4% of the total volume for sizes from 115 ± 65 nm). In experiment 3 the size distribution is more continuous, and the difference between the smaller and larger size group is not as apparent, as there is no clear gap between the peaks. However, a greater volume of Au is used up for the larger nanoparticles ranging from 40–120 nm (Fig. 4; Exp. 3, 83.9% of the total volume). This probably occurs since the DTP mechanism is more dominant than the GTP mechanism and a greater volume of the dissolved Au from the precursor is used to generate particles from the droplet, instead of generating the particles from the gas phase.

In regard to the formation mechanisms, a higher Au concentration allowed a bigger portion of AuNPs to be formed via the DTP mechanism:

Exp. 1: Conc.: 2.5 g/l Au, 96.4% of the total volume used up for larger AuNPs;

Exp. 2: Conc.: 1.25 g/l Au, 92.4% of the total volume used up for larger AuNPs;

Exp. 3: Conc.: 0.625 g/l Au, 83.9% of the total volume used up for larger AuNPs (from 40 to 120 nm).

The nanoparticle sizes are bigger for experiments with a higher starting Au precursor solution concentration, which is to be expected. This is apparent for both GTP and DTP mechanisms (Figs. 2 and 3). In Exp. 2, the smaller nanoparticles, produced via GTP, have very small sizes (11 ± 7 nm) in high numbers; this indicates that more seeds were formed from the gas phase, which did not grow into bigger nanoparticles due to material depletion. The GTP mechanism presence increases with lower Au precursor concentrations (which is also confirmed by the volume % used up for larger nanoparticles). Due to a more heterogeneous precipitation from the liquid phase during evaporation, more material is then formed into the gas phase and GTP has more influence the final nanoparticle sizes.

In Exp. 3 (Fig. 4) the sizes of the nanoparticles, obtained through GTP mechanism should be even lower, due to the use of the lowest Au precursor solution concentration (0,625 Au g/l). However, the nanoparticles produced by the GTP mechanism are overlapping the ones produced via DTP, and the two size ranges are difficult to distinguish. This suggests that the gas phase from the GTP mechanism has very low vapor pressures and is mainly being used up for growth of the smaller nanoparticles, which were produced by DTP.

The occurrence of this combination of formation mechanisms suggests unfavorable conditions for a controlled synthesis of AuNPs. This indicates that during the evaporation in the first heating zone of the synthesis, partially dried droplets of the starting solution are produced. These are then evaporated rapidly in the second heating zone, producing unfavorable results (bimodal size distribution). The calculations used for the first heating zone temperature are not suitable for our type of experimental approach.[22, 26] The use of higher evaporation temperatures produces an unfavorable rapid evaporation of droplets in the length of the given evaporation zone (28 cm).

After the initial precursor solution droplets ($HAuCl_4$ with water) are created, they are transported inside the first heating zone. In this zone, the water is evaporated, raising the relative humidity in the system, as more water vapor is present. At higher levels of relative humidity the droplets evaporate more slowly, because of the increased partial vapor pressure around the droplet. This results in droplets not evaporating fully, forming partially dried droplets. These partially dried droplets then enter the second heating zone, where the reactions take place. Inside the second heating zone, the droplets enter an environment of relatively high temperatures, increasing the droplet

temperature rapidly. The remaining water then evaporates fast, not giving time for diffusion of the solute into the center of the droplet. This produces a combination of a particle and vapor of gold chloride from the droplet. From this point, there are several further occurrences that formed the final nanoparticles (Fig. 6):

1. Particles formed from a droplet were collected in the washing bottles (DTP mechanism)
2. Particles formed from a droplet collided with other particles formed from a droplet, promoting growth, and these were then collected in the washing bottles (DTP mechanism)
3. Particles formed from a droplet collided with vapor, promoting growth, and were then collected in the washing bottles (DTP and GTP mechanisms)
4. Vapor molecules collided with other vapor molecules resulting in the nucleation of a new particle (GTP mechanism).

3.3. Electron Diffraction

Electron diffraction was conducted on the samples for a better understanding of the crystal structure and particle growth from DTP and GTP mechanisms. The electron diffraction has shown a space group Fm-3m in the samples, which corresponds to a face centered cubic lattice structure present in the gold (Fig. 7).

The surface energies of the Au face centered cubic lattice are as follows:[32] $a_{\{111\}} < a_{\{100\}} < a_{\{110\}}$. No apparent grain orientation is present (some possible growth directions are presented in Fig. 7(a) of a singular particle). This suggests that the growth of the nanoparticles is heterogeneous. This is in agreement with the nanoparticle formation mechanisms from aerosol droplets, as the smaller particles formed from the gas phase by GTP grow from nuclei in several directions. Larger particles formed by DTP, show heterogeneous growth due to several nucleation sites within the aerosol droplet. Particles initially formed by DTP and later enlarged via GTP also do not exhibit homogeneous growth, which is in compliance with this type of nanoparticle. A simulation of the crystal lattice is also presented in Figure 7.

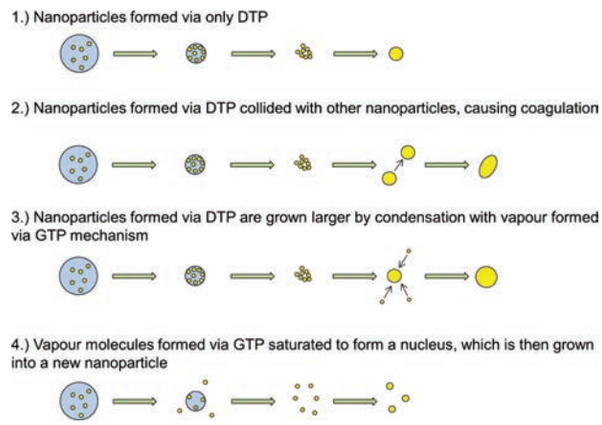

Fig. 6. AuNP formation modes with a combination of DTP and GTP mechanisms in USP.

3.4. Cytocompatibility Results

Previously we showed that pure AuNPs generated by USP are not cytotoxic for L929 cells, rat thymocytes[25] and splenocytes, up to the concentration of 100 μg/ml. In contrast, the toxicity of AuNPs contaminated with the alloying elements increased with the decreased amount of Au per nanoparticles.[24, 25] Here we used different concentrations of $HAuCl_4$ as precursor solutions for AuNP synthesis by USP, which resulted in the production of only pure AuNPs (99 wt%). Furthermore, we wondered whether the bimodal size distribution of AuNPs produced by the reconstructed USP, affect the cell viability and functions.

Upon the synthesis of AuNPs, we tested whether these nanoparticles are cytocompatible. To evaluate this, AuNPs were cultivated with L929 cells at different concentrations (12 μg/ml–100 μg/ml) for up to 48 h. After the cultivation, the internalization of AuNPs by L929 cells was analyzed, as well as the viability, apoptosis and proliferation of cells in the cultures, as described in Materials and Methods.

Phase-contrast microscopy of L929 cells in the cultures suggested that these cells internalize all three types of AuNPs, but the quantity of the internalized AuNPs seems dependent on the AuNP type (Fig. 8(a)) and the applied concentration. The level of internalization of AuNPs increased with the higher concentrations of AuNPs applied in the cultures (data not shown). The highest level of accumulation in L929 cells was observed for AuNPs in exp. 3, whereas the uptake of AuNP in exp. 2 was lowest.

The viability assay suggested that neither type of AuNPs induces L929 cell death at concentrations up to 100 μg/ml, since the percentages of viable cells were similar between control and those cells treated with AuNPs (Fig. 8(b)). A similar finding was observed by analyzing the percentage of L929 cells with the hypodiploid DNK content, suggesting that AuNPs produced by USP do not induce apoptosis of L929 cells at the applied concentrations (Fig. 8(c)). These results are in line with our previous results.[24, 25] Additionally, we also showed,[33] along with the other studies,[34] that pure AuNPs produced by chemical methods also do not cause significant toxicity if applied in similar concentrations. One of the reasons for the low cytotoxicity of AuNPs could be due to the fact that Au ions are hardly releasable in a culture medium.[35] However, even pure AuNPs are not completely inert in culture conditions.

Previously, we showed that the higher concentrations of (100 μg/ml) were able to inhibit the proliferation capacity of L929 cells,[25] as well as the proliferation of splenocytes induced by ConA,[24] and such effect was potentiated additionally by AuNPs which were smaller in diameter. However, these results do not allow predicament of

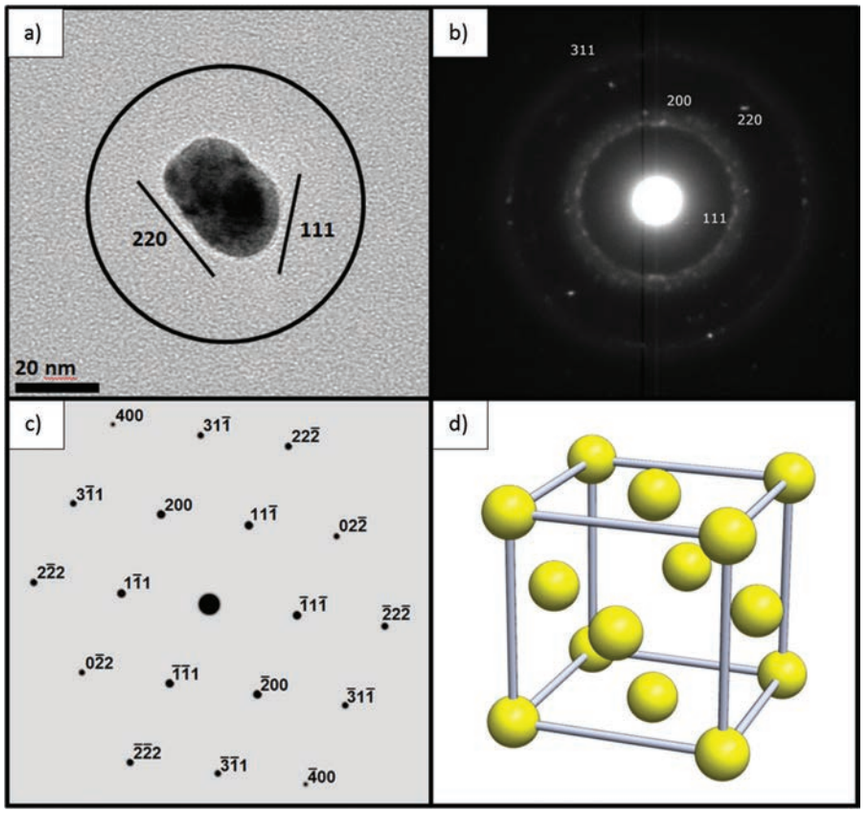

Fig. 7. Electron diffraction on the synthesized singular AuNP with a crystal lattice simulation; (a) TEM micrograph of a single AuNP with visible selected site of electron diffraction (b) electron diffraction of a single AuNP (c) crystal lattice simulation, space group Fm-3m (d) representation of a face centered cubic lattice structure.

AuNPs effects on proliferation, just based on their size distribution. Therefore, we analyzed the ability of L929 cells to proliferate in the presence of increasing concentrations of AuNPs for 48 h (Fig. 8(d)). AuNPs obtained from all three experimental setups did not modulate the proliferation capacity of L929 cells at concentrations lower that 100 μg/ml. At the highest concentration applied, the AuNPs in exp. 1 and AuNP in exp. 2 also did not affect the proliferation of L929 cells, whereas the proliferation of cells in the culture with AuNPs in exp. 3 was found to be significantly lower than the proliferation in control cultures.

A possible explanation for this phenomenon could be the specific size distribution of AuNPs. Namely, the AuNP in exp. 1 had a similar amount of the nanoparticles sized about 40 nm and those higher than 100 nm. The AuNP in exp. 2 had a much higher amount of smaller nanoparticles (7 nm), and only a few percentages of those sized 50–170 nm, whereas the AuNP in exp. 3 had almost all nanoparticles smaller than 100 nm. Chithrani et al.[36] showed, using HeLa cells as the model system that AuNPs sized around 50 nm are taken up by the cells in higher levels compared to AuNPs smaller or larger in diameter. A similar finding was confirmed by Lu et al.,[37] which used mesoporous silica nanoparticles. Such size-dependent preferences in nanoparticles' uptake also correlate with the uptake dynamics. Namely, Rejman et al.[38] reported that the saturation time increases with nanoparticles' size, from 30 min (for 50–100 nm beads) to several hours (200 nm beads). Based on these results, it could be expected that the nanoparticles smaller than 100 nm are taken up faster and in higher amounts than the nanoparticles larger than 100 nm. However, this cannot explain why the AuNPs in exp. 2 were internalized by L929 to a lesser extent than the other AuNPs. It should be noted, however, that the smaller nanoparticles require clustering to enter the cells.[39] These authors showed that single 50 nm sized transferring-coated AuNPs are able to induce the formation of endocytic vesicles, whereas at least 6 nanoparticles sized 14 nm need to form a cluster on the cell membrane to enter the cells. Jin et al.[40] suggested that nanoparticles smaller in size have to cluster on the cell membrane to form a size sufficient to generate a large enough enthalpic contribution via receptor ligand interaction to overcome the elastic energy and entropic barriers associated with vesicle formation. Cumulatively, it could be expected that the AuNPs in exp. 1 and AuNPs in exp. 2 are internalized to a lesser extent due to the higher percentage of AuNPs sized over 100 nm and high percentage of AuNPs smaller in size (7 nm), respectively. Alternatively, the size-dependent

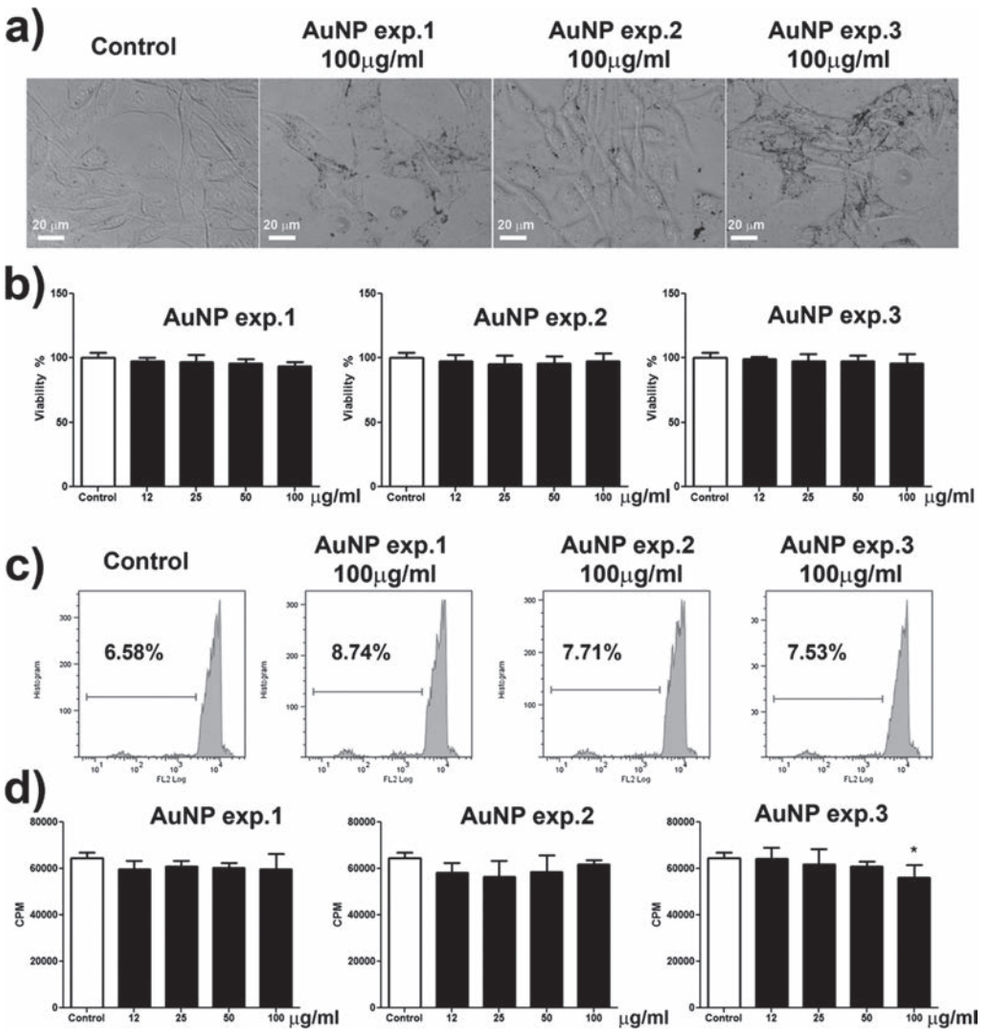

Fig. 8. Cytocompatibility of AuNPs produced by USP; (a) Phase contrast microscope analyze of L929 cells cultivated alone (Control), or in the presence of AuNPs (100 μg/ml) produced in three different experimental setups, for 48 h. (b) Viability of L929 cells cultivated in the presence of different concentrations of AuNPs, or alone (Control) for 48 h. The results, expressed as the percentage of viable cells of control (100%), are presented as the mean viability $\pm$ SD of sixplicates. (c) Apoptosis of L929 cells cultivated alone (Control) or in the presence of AuNPs (100 μg/ml) for 48 h. After the culture, the cells were stained with PI/hypotonic solution and analyzed by flow cytometry. A representative experiment is shown, out of three with similar results. (d) Proliferation of L929 cells cultivated alone (Control), or in the presence of different doses of AuNPs for 48 h. The results are expressed as the mean CPM $\pm$ SD of sixplicates. $^{*}p < 0.05$ compared to control (one way ANOVA).

sedimentation rate of AuNPs in culture,[41] might have led to a different availability of AuNPs to the adherent L929 cells, and therefore, different internalization. Whatever the reason, our microscopy analyze confirmed that the AuNPs in exp. 3 are best internalized by L929 cells, which might explain why these nanoparticles exhibited an anti-proliferative potential when applied in high concentrations (100 μg/ml), unlike other AuNPs. At present it is not known what the mechanism is behind the anti-proliferative potential of the AuNPs in exp. 3. Gold is one of the most electronegative metals we know, which was found to interact with various SH containing groups, including the cell proteins such as cathepsins,[42] HMBG-1[43] actin filaments[44] and many others. Therefore, to narrow down the search for the observed phenomenon of Au in exp. 3, a more detailed study on their cellular internalization and cellular trafficking is needed in the future.

4. CONCLUSIONS

The parameter selection for the modular redesign of USP has yielded AuNP formation with bimodal size distributions, which can be attributed to a combination of DTP and GTP formation mechanisms. The DTP mechanism was shown to be more dominant in the process. In order to ensure that only the DTP formation mechanism takes place and disable the formation of bimodal nanoparticle size distributions, the evaporation should be optimized with different temperatures and evaporation zone length.

The modular redesign of USP in comparison with conventional USP seems to improve the morphologies of the AuNPs, as mainly spherical and some irregular nanoparticle shapes were produced.

The cytocompatibility study has shown that the AuNPs produced with the modular USP redesign are not cytotoxic for L929 cells. However, these nanoparticles can exhibit the anti-proliferative effects if applied in higher concentrations, which depends predominantly on their size distribution.

Acknowledgment: The research was carried out under the Young Researcher Program funded by the Slovenian Research Agency (ARRS) and the Project L2-4212: "Gold nanoparticle production technology."

References and Notes

1. E. Boisselier and D. Astruc, *Chem. Soc. Rev.* 38, 1759 (**2009**).
2. H. Jans, X. Liu, L. Austin, G. Maes, and Q. Huo, *Anal. Chem.* 81, 9425 (**2009**).
3. J. A. Ryan, K. W. Overton, M. E. Speight, C. N. Oldenburg, L. Loo, W. Robarge, S. Franzen, and D. L. Feldheim, *Anal. Chem.* 79, 9150 (**2007**).
4. M. Shah, V. D. Badwaik, and R. Dakshinamurthy, *J. Nanosci. Nanotechnol.* 14, 344 (**2014**).
5. L. Sun, D. Liu, and Z. Wang, *Langmuir* 24, 10293 (**2008**).
6. L. Xu, Y. Zhu, W. Ma, W. Chen, L. Liu, H. Kuang, L. Wang, and C. Xu, *J. Phys. Chem. C* 115, 3243 (**2011**).
7. D. Pissuwan, C. H. Cortie, S. M. Valenzuela, and M. B. Cortie, *Trends in Biotech.* 28, 207 (**2010**).
8. X. Huang and M. A. El-Sayed, *J. Adv. Res.* 1, 13 (**2010**).
9. A. Kumar, B. M. Boruah, and X.-J. Liang, *J. Nanomat.* 2011, 1 (**2011**).
10. A. J. Mieszawska, W. J. M. Mulder, Z. A. Fayad, and D. P. Cormode, *Mol. Pharm.* 10, 831 (**2013**).
11. H. Zhao, L. Lin, J. Li, J. Tang, M. Duan, and L. Jiang, *J. Nanopart. Res.* 3, 321 (**2001**).
12. A. Y. Lin, J. P. M. Almeida, A. Bear, N. Liu, L. Luo, A. E. Foster, R. A. Drezek, and T. W. Prow, *PLoS ONE* 8, e63550 (**2013**).
13. J. Turkevich, P. C. Stevenson, and J. Hillier, *Discuss. Faraday Soc.* 11, 55 (**1951**).
14. A. Lähde, I. Koshevoy, T. Karhunen, T. Torvela, T. A. Pakkanen, and J. Jokiniemi, *J. Nanopart. Res.* 16, 2716 (**2014**).
15. Y.-C. Wang and S. Gunasekaran, *J. Nanopart. Res.* 14, 1200 (**2012**).
16. R. Rudolf, P. Majeric, S. Stopic, J. Bogovic, M. Colic, S. Tomic, M. Jenko, and B. Friedrich, *Mat. Tech.* 47, 577 (**2013**).
17. B. Janković, S. Stopić, J. Bogović, and B. Friedrich, *Chem. Eng. Proc.: Process Intensification* 82, 71 (**2014**).
18. J. Bogovic, R. Rudolf, and B. Friedrich, *JOM* 67, 1 (**2015**).
19. K. Okuyama and I. W. Lenggoro, *Chem. Eng. Sci.* 58, 537 (**2003**).
20. W. H. Suh, A. R. Jang, Y.-H. Suh, and K. S. Suslick, *Adv. Mater.* 18, 1832 (**2006**).
21. P. S. Patil, *Mat. Chem. Phys.* 59, 185 (**1999**).
22. T. T. Kodas and M. J. Hampden-Smith, Aerosol Processing of Materials, Wiley-VCH, New York (**1999**)..
23. F. Iskandar, A. Mikrajuddin, and K. Okuyama, *Nano. Lett.* 1, 231 (**2001**).
24. J. Đokić, R. Rudolf, S. Tomić, S. Stopić, B. Friedrich, B. Budič, I. Anžel, and M. Čolić, *J. Biomed. Nanotechnol.* 8, 528 (**2012**).
25. R. Rudolf, B. Friedrich, S. Stopic, I. Anzel, S. Tomic, and M. Colic, *J. Biomat. Appl.* 26, 595 (**2012**).
26. Y. Xiong and T. T. Kodas, *J. Aerosol Sci.* 24, 893 (**1993**).
27. G. V. Jayanthi, S. C. Zhang, and G. L. Messing, *Aerosol. Sci. Tech.* 19, 478 (**1993**).
28. P. Majeric, R. Rudolf, and B. Friedrich, *Mat. Tech.* 49, 791 (**2015**).
29. C. A. Schneider, W. S. Rasband, and K. W. Eliceiri, *Nat. Meth.* 9, 671 (**2012**).
30. M. Eslamian, M. Ahmed, and N. Ashgriz, *Drying Tech.* 27, 3 (**2009**).
31. J. Bogovic, S. Stopic, B. Friedrich, and J. Schroeder, Nanosized metallic oxide produced by Ultrasonic Spray Pyrolysis, *Proceedings of European Metallurgical Conference EMC 2011*, Düsseldorf, Germany, June (**2011**).
32. P. Pallavicini, A. Dona`, A. Casu, G. Chirico, M. Collini, G. Dacarro, A. Falqui, C. Milanese, L. Sironi, and A. Taglietti, *Chem. Commun.* 49, 6265 (**2013**).
33. S. Tomić, J. Đokić, S. Vasilijić, N. Ogrinc, R. Rudolf, P. Pelicon, D. Vučević, P. Milosavljević, S. Janković, I. Anžel, J. Rajković, M. S. Rupnik, B. Friedrich, M. Čolić, and S. Hussain, *PLoS ONE* 9, e96584 (**2014**).
34. N. Khlebtsov and L. Dykman, *Chem. Soc. Rev.* 40, 1647 (**2011**).
35. M. Colic, D. Stamenkovic, I. Anzel, G. Lojen, and R. Rudolf, *Gold Bull.* 42, 34 (**2009**).
36. B. D. Chithrani, A. A. Ghazani, and W. C. W. Chan, *Nano Lett.* 6, 662 (**2006**).
37. F. Lu, S.-H. Wu, Y. Hung, and C.-Y. Mou, *Small* 5, 1408 (**2009**).
38. J. Rejman, V. Oberle, I. S. Zuhorn, and D. Hoekstra, *Biochem. J.* 377, 159 (**2004**).
39. B. D. Chithrani and W. C. W. Chan, *Nano Lett.* 7, 1542 (**2007**).
40. H. Jin, D. A. Heller, R. Sharma, and M. S. Strano, *ACS Nano.* 3, 149 (**2009**).
41. E. C. Cho, Q. Zhang, and Y. Xia, *Nature Nanotech.* 6, 385 (**2011**).
42. J. L. Speshock, L. K. Braydich-Stolle, E. R. Szymanski, and S. M. Hussain, *Nanoscale Res. Lett.* 146, 169 (**2010**).
43. C.-Y. Tsai, S.-L. Lu, C.-W. Hu, C.-S. Yeh, G.-B. Lee, and H.-Y. Lei, *The Journal of Immunology* 188, 68 (**2011**).
44. R. Coradeghini, S. Gioria, C. P. García, P. Nativo, F. Franchini, D. Gilliland, J. Ponti, and F. Rossi, *Toxicology Lett.* 217, 205 (**2013**).

Received: 24 September 2015. Accepted: 31 October 2015.